Lasers in Manufacturing Conference 2019

Numerical investigations of the temperature distribution around the capillary and its effect on the stability of the capillary rear wall

Peter Berger[a]*

[a]*Institut für Strahlwerkzeuge (IFSW), Universität Stuttgart, Pfaffenwaldring 43, 70569 Stuttgart, Germany*

Abstract

For some years now, three-dimensional numerical investigations have been used to gain insights into many phenomena of laser beam welding. However, two-dimensional investigations may be better suited to clarify basic interaction phenomena. The problem to be particularly emphasized here is welding at high speed and with relatively large capillaries. The influence of different parameters on the shape of the weld pool is shown, including the influence of different material properties at different Péclet numbers. Different flow conditions around and behind the capillary are also considered. As a result, it was found that at high Péclet numbers zones with high temperatures and low temperature gradients occur behind the capillary. These can destabilize the capillary back wall, which could explain the transition from a circular to an elongated capillary with increased welding speed.

Keywords: Laser-beam welding; capillary; stability; numerical simulation

* Corresponding author. Tel.: +49-711-686-66843; fax: +49-711-685-6842.
E-mail address: peter.berger@ifsw.uni-stuttgart.de.

1. Introduction

In laser beam welding two major regimes are known: *conduction mode welding* and *deep-penetration welding*. Particularly in deep penetration welding, however, several more variants of the welding process can be identified depending on the selected parameters. Whereas some variants connected with certain phenomena, e.g. humping and pore generation, could be attributed to specific parameter regimes since a long time, Fabbro et al, 2007 described a more systematic classification of a large parameter region in the deep-penetration welding regime. They named five regimes depending on two parameters, namely the laser power and the welding speed (Fig. 1). They called the first regime at low welding speed *"Rosenthal" regime*, which is characterized by a well-defined and circular keyhole and a weld pool showing very important chaotic oscillations. When increasing the welding velocity, it is followed by the second regime called *single wave regime*. The typical feature in this regime is a single swelling generated near the top of the rear keyhole wall. The *elongated keyhole regime* is the third regime and is characterized by an elongated keyhole whose length fluctuates. Regimes number four and five (*pre-humping* and *humping regime*) are characterized by an inclined keyhole front wall and an elongated keyhole and a significant amount of melt emerging from the bottom of the front keyhole wall. The *humping regime* differs from all other regimes by a characteristic seam shape with strong undercuts and periodic large swellings along the upper seam surface.

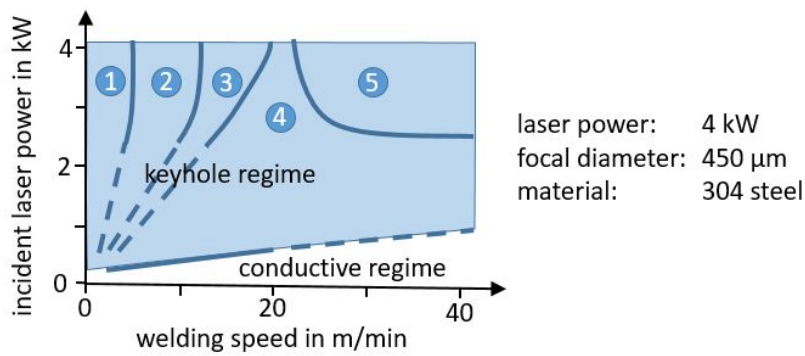

Fig. 1. Regimes after Fabbro et al., 2007 with data from Fabbro, 2011; for deep-penetration welding Fabbro et al., 2007 identified five regimes: (1) "Rosenthal" regime, (2) single wave regime, (3) elongated keyhole regime, (4) pre-humping regime and (5) humping regime; the solid lines follow data points given in Fabbro, 2011; the dashed lines are extrapolations from these data points.

In the past and still today, many processes are carried out in the first two systems. With the development of lasers with more and more power, welding in the elongated keyhole regime becomes more and more interesting, as the high laser power can be converted into high speed, while at even higher speeds the fifth regime is reached, which must be avoided because of the very poor seam quality. It therefore seems interesting to take a closer look at the transition from the second to the third regime. This transition can easily be observed using X-ray technology when welding aluminum (Fig. 2). In contrast to steel, the transition speed of aluminum welding is somewhat higher (compare Fig. 2 with Fig. 1).

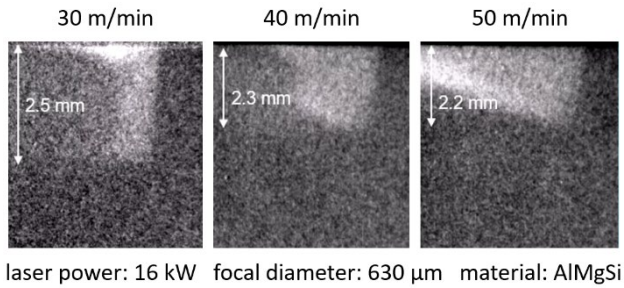

Fig. 2. Three capillaries during welding of AlMgSi with 16 kW laser power and a focal diameter of 630 µm, observed by X-ray technique; Fetzer et al., 2018

Already in Fabbro et al., 2007 an indication was given as to what is causing this transition. In that paper a collision of the vapor plume, emitted from the keyhole front, with the rear side of the capillary is described. Reflections of the laser radiation from the front to the rear side are also mentioned. In principle, this reflected light can cause evaporation at the rear capillary wall, which pushes the capillary backwards. Fabbro et al, 2007 do not exclude reflections, but admit that they are small after Fabbro et al, 2005.

In Berger et al., 2015, the influence of the laser radiation on capillary shapes alone – neglecting the transfer of vapor from the front to the rear side of the capillary – could be demonstrated using numerical calculations. In that paper calculated shapes of capillaries in iron workpieces for different welding speeds were shown. A strong bending of the capillary and bulging of its rear side could be observed at high welding speeds (15 and 20 m/min). It could thus be shown that the back pressure generated by the evaporation of heavily irradiated areas on the back of the capillary is capable of creating bulges in these capillary areas.

A third possibility could be an energy transfer by the vapor jet. If a part of this jet condenses on the rear wall, the evaporation energy is released. If, however, the temperature gradients in the surrounding of the capillary are small and the temperature is close to evaporation temperature, this energy cannot be transferred to the workpiece by conduction or convection and, therefore, part of the vapor cannot condense, which increases the pressure in the capillary. An indication of this process was given in Fabbro et al., 2007, where it was mentioned that warming could be observed in a region where the plume emerging from the front hits the elongated keyhole. In order to investigate the temperature gradients in the capillary's surrounding, numerical simulations have been performed.

2. Temperature distributions around the capillary calculated by a 2-D numerical model

During the numerical solution, the time-dependent 2-D heat equation

$$\dot{q}_{3\mathrm{d}} = \rho \cdot c_p \cdot \frac{\partial T}{\partial t} + \nabla\left(\rho \cdot c_p \cdot T \cdot \vec{u}\right)$$

was solved with the aid of an explicit scheme ($\dot{q}_{3\mathrm{d}}$ being the heat source, T the temperature and t the time). The material properties of iron were used. The density ρ and the thermal heat conductivity λ_{th} were chosen temperature-dependent. The specific heat c_p was either constant or it was also treated in dependence of the temperature. In the latter case, also the latent heat of fusion and the heat of transformation from beta to gamma iron were included. A rectangular grid with 800000 points was used.

The material velocity $\vec{u}$ was either constant over the entire metal plate, including the capillary, or a flow field was calculated around the capillary. In this case, a linear velocity change from the melting isotherm to the evaporation isotherm was prescribed with zero velocity inside the capillary. To investigate the effect of a

three dimensional eddy in the weld pool behind the capillary, the velocity components of the 2-D simulation were overlaid by such a 3-D eddy.

Results are shown in Figures 3 to 6. Comparing the temperature fields from calculations with and without the latent heat of fusion, a strong influence can be identified in the solidification area. An example for a welding with a Péclet number of 1.875 is shown in Fig. 3 (The Péclet number was calculated from the product of the capillary diameter and the welding speed divided by the thermal diffusivity; for steel an average value of $8 \cdot 10^{-6}$ m²/s was chosen). In the region close to the capillary, however, only a small influence can be observed. This can be clearly seen when comparing the calculated temperature distributions in the symmetry planes of the weld seams. (Fig. 4).

Comparing the gradients in the temperature field in the symmetry line behind the capillary when changing the Péclet number, one finds, however, a significant decrease of this gradient with an increase of the Péclet number (Fig. 5). This flattening of the temperature field directly behind the capillary indicates that less and less additional heat, which could be released at the back of the capillary, can be transferred to the bulk material (in addition to Fig. 5 compare the isotherms in Fig. 3 and Fig. 6).

This effect can be modified by changing the fluid flow around and behind the capillary. Different flow situations are illustrated in Fig. 7. Here the material flow in the symmetry line is shown for three different assumptions: (1) movement of plate only, (2) regarding the melt flow around the capillary and (3) overlaying the flow field of a 3-D eddy in addition to the flow around the capillary.

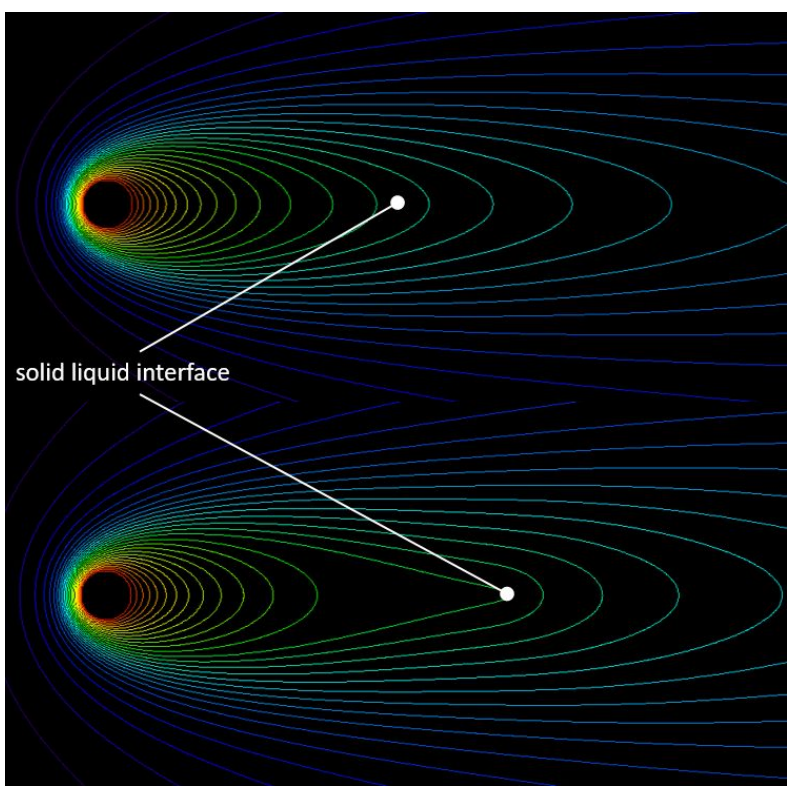

Fig. 3. Calculated isotherms for a welding at Péclet number 1.875 (capillary radius: 50 µm; welding speed: 0.15 m7s; top: heat of fusion was neglected; bottom: heat of fusion was taken into account

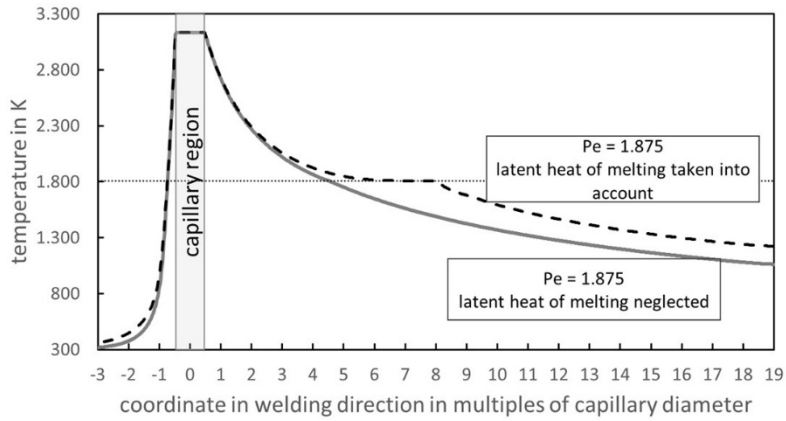

Fig. 4. Two calculated temperature distributions along the symmetry plane of a welding at a Péclet number of 1.875 (capillary radius: 50 µm, welding speed: 0.15 m/s); dashed line: the latent heat of fusion was taken into account; gray solid line: the latent heat of melting was neglected; the melting temperature at 1807.15 K is indicated by a dotted line

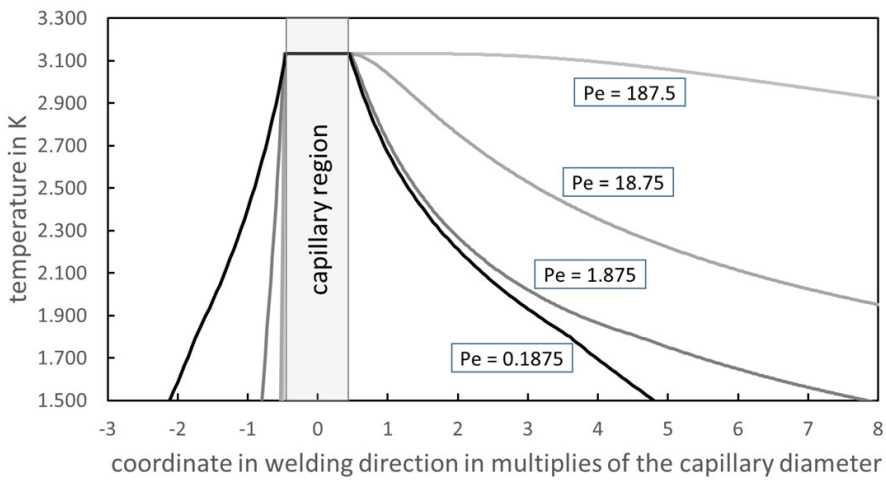

Fig. 5. Four calculated temperature distributions along the symmetry plane of weld seams at Péclet numbers from 0.1875 to 187.5 (for the three lower Pe numbers the capillary radius is 50 µm, welding speeds 0.015, 0.15, and 1.5 m/s, at Pe = 187.5 the capillary radius is 500 µm and a welding speed of 1.5 m/s):)

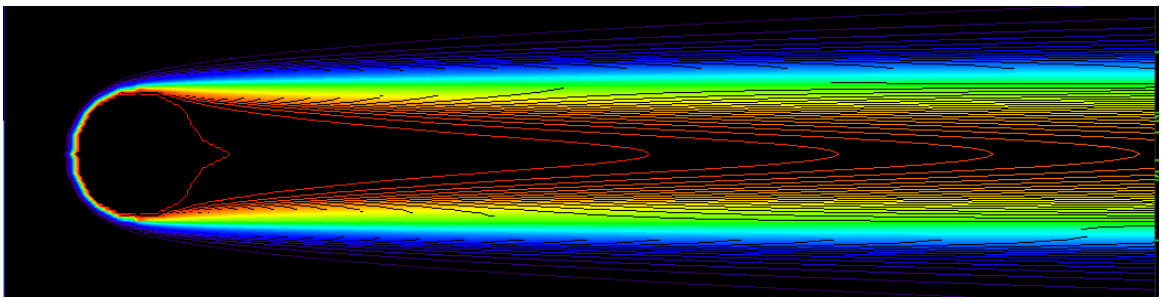

Fig. 6. Calculated isotherms for a weld seam at Péclet number 187.5 (capillary radius: 500 µm; welding speed: 1.5 m/s; heat of fusion was not taken into account; isotherms every 50 K)

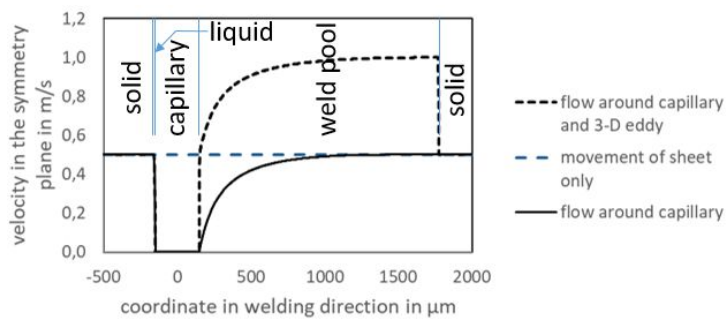

Fig. 7. Velocity of the material in the symmetry plane of the weld; calculated for a welding at Péclet number 125 (capillary radius: 150 µm; welding speed: 0.5 m/s; heat of fusion was not taken into account

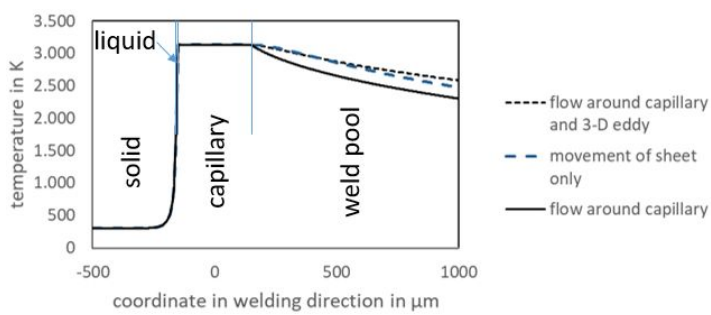

Fig. 8. Temperature distribution in the symmetry plane of the weld; calculated for a welding at Péclet number 125 (capillary radius: 150 µm; welding speed: 0.5 m/s; heat of fusion was not taken into account (same conditions as in Fig. 5)

Fig. 8 shows that the assumed flow field around the capillary increases the temperature gradient, while a high-speed flow away from the capillary leads to an additional decrease in the temperature gradient. However, the presented influence of the Péclet number (Fig. 5) is much greater than that of the flow changes shown in Figs. 7 and 8.

3. Conclusion

Following the definitions of regimes in deep-penetration welding given by Fabbro et. al, 2007, three possible reasons seem to be plausible for the transition from regime 2 to 3:

- a jet of vapor emerging from the front and transferring momentum to the rear side,
- laser radiation reflected from the front causing evaporation at the rear side, and
- the above mentioned jet, which transmits energy by evaporation at the front and condensation at the rear of the capillary, where part of the vapor may not be able to condense , thus increasing the pressure.

A large temperature gradient is necessary to transfer the energy released at the rear side of the capillary into the workpiece. This gradient, however, is significantly reduced with increasing Péclet number. Additionally, a strong flow eddy behind the keyhole inducing a fluid flow away from the capillary increases the effect of lowering the temperature gradients.

Acknowledgements

The presented work was funded by the Deutsche Forschungsgemeinschaft (DFG, German Research Foundation) - Projektnummer 266218804. The responsibility for this paper is taken by the author.

References

Berger, P., Heider, A., Boley, M., Förster, D., 2015. Capillary geometries during welding of metals observed with X-ray technique and calculated using a ray-tracing tool and a finite volume program treating heat diffusion and fluid flow, LIM 2015.

Fabbro, R., Slimani, S., Coste, F., Briand, F., 2005. Study of keyhole behavior for full penetration Nd-Yag CW laser welding, J. Phys. D: Appl. Phys. 38, p. 1881-1887.

Fabbro, R., Slimani, S., Coste, F., Briand, F., 2007. Analysis of the various melt pool hydrodynamic regimes observed during cw Nd-YAG deep penetration laser welding, The International Congress on Applications of Lasers & Electro-Optics (ICALEO) 2007, paper 802.

Fabbro, R., 2011. Review on process regimes in laser welding of metals - What do we know exactly? presenation at the 25th anniversary celebration of the IFSW.

Fetzer, F., Hagenlocher, Ch. and Weber,R., 2018, High power, high speed, high quality: advantages of laser beam welding of aluminum sheets at 16 kW of laser power and feed rates up to 50 m/min, Laser Technik Journal 15.3, p. 28-31.